

# Strong coupling constant extraction from high-multiplicity $Z + \text{jets}$ observables

Mark Johnson\*

*School of Physics and Astronomy, The University of Manchester, Manchester M12 9PL, United Kingdom  
and The Cockcroft Institute, Sci-Tech Daresbury, Warrington WA4 4AD, United Kingdom*

Daniel Maître†

*Institute for Particle Physics Phenomenology, Ogden Centre for Fundamental Physics,  
Department of Physics, University of Durham, Science Laboratories,  
South Road, Durham DH1 3LE, United Kingdom*



(Received 18 December 2017; published 15 March 2018)

We present a strong coupling constant extraction at next-to-leading order QCD accuracy using ATLAS  $Z + 2,3,4$  jets data. This is the first extraction using processes with a dependency on high powers of the coupling constant. We obtain values of the strong coupling constant at the  $Z$  mass compatible with the world average and with uncertainties commensurate with other next-to-leading order extractions at hadron colliders. Our most conservative result for the strong coupling constant is  $\alpha_s(M_Z) = 0.1178_{-0.0043}^{+0.0051}$ .

DOI: [10.1103/PhysRevD.97.054013](https://doi.org/10.1103/PhysRevD.97.054013)

## I. INTRODUCTION

The strong coupling constant  $\alpha_s$  is a physical parameter of QCD that cannot be predicted from first principles and has to be obtained from an experimental measurement. Values of  $\alpha_s$  have been previously obtained by comparing experimental data from hadronic  $\tau$  decays, deep inelastic scattering, heavy quarkonia decays, or measurements from  $e^+e^-$  and hadron colliders against theoretical predictions from perturbative or lattice QCD (for a review, see Ref. [1]). These different extractions have different levels of sensitivity depending on the order at which the  $\alpha_s$  expansion of the observable starts. This order is  $\alpha_s^0$  for extractions based on the  $R$  ratio. Three-jet rates and event shapes at  $e^+e^-$  use observables of which the expansion starts at order  $\alpha_s^1$ . At hadron colliders, the ratio of three jet production to two jet production [2] and the transfer energy-energy correlation [3] starts at order  $\alpha_s^1$ , and the inclusive jet cross section [4] starts at order  $\alpha_s^2$ . The five-jet production rates at LEP [5], the heavy quarkonia hadronic decay width [6], and the three-jet inclusive observables [7] are the observables with the highest sensitivity used so far; their expansion starts at order  $\alpha_s^3$ . Typically, the increased sensitivity comes at a cost,

as observables with a lower sensitivity to  $\alpha_s$  can be measured more precisely than those with a higher dependency. In this work, we present an extraction of  $\alpha_s$  using  $Z + 2, 3, 4$  jets differential cross section measurements from the ATLAS Collaboration [8] at a center-of-mass energy of 7TeV, comparing them to next-to-leading order (NLO) predictions from BLACKHAT+SHERPA [9] which start at orders  $\alpha_s^2$ ,  $\alpha_s^3$ , and  $\alpha_s^4$  respectively. The increased sensitivity of the higher-multiplicity observables partly compensates the larger experimental and theoretical uncertainties in such a way that the three different multiplicities yield comparable degrees of precision for the  $\alpha_s$  extraction. We combine the three multiplicities to obtain a final value for  $\alpha_s(M_Z)$ .

## II. EXTRACTION PROCEDURE

To obtain our  $\alpha_s$  value, we compare theoretical predictions obtained from the BLACKHAT+SHERPA Collaboration [9] with ATLAS data. We minimize the  $\chi^2$  function

$$\chi^2(\alpha_s(M_Z)) = (y_t(\alpha_s(M_Z)) - y_d)^T C^{-1} (y_t(\alpha_s(M_Z)) - y_d), \quad (1)$$

where  $y_t$  are the predictions from theory and  $y_d$  are the experimental values. The covariance matrix  $C$  is given by

$$C = C_{\text{exp}} + C_{\text{pdf}} + C_{\text{theory}}, \quad (2)$$

where  $C_{\text{exp}}$  is the experimental error covariance matrix, described in Sec. II D and  $C_{\text{pdf}}$  and  $C_{\text{theory}}$  are the parton distribution function (PDF) and theory statistical uncertainty covariance matrices, which we describe in detail in Sec. II A.

\*mark.andrew.johnson@cern.ch

†daniel.maitre@durham.ac.uk

*Published by the American Physical Society under the terms of the Creative Commons Attribution 4.0 International license. Further distribution of this work must maintain attribution to the author(s) and the published article's title, journal citation, and DOI. Funded by SCOAP<sup>3</sup>.*

Our best fit value  $\alpha_0$  for  $\alpha_S(M_Z)$  is the value that minimizes  $\chi^2$ , and the  $1 - \sigma$  interval is given by the values  $\alpha_{\pm}$  of  $\alpha_S(M_Z)$  corresponding to  $\chi^2(\alpha_{\pm}) = \chi^2(\alpha_0) + 1$ .

In addition to the sources of uncertainty listed above, we also consider theoretical uncertainties due to the factorization and renormalization scale variation and the nonperturbative corrections. These uncertainties affect the fit through a rescaling of the theoretical prediction and corresponding covariance matrix  $C_{\text{theory}}$ . They are described in more details in Secs. II B and II C.

To obtain the values  $y_i(\alpha_S(M_Z))$ , we need to perform a consistent calculation of the theoretical prediction using the same value of  $\alpha_S(M_Z)$  in the hard matrix elements as the one used to fit the PDFs. This is possible since many PDF fitting groups provide dedicated fits performed with a range of value of  $\alpha_S(M_Z)$ . This gives us a discrete set of values for  $\chi^2(\alpha_S)$ , and in order to obtain the precise values of the minimum and  $1 - \sigma$  interval, we fit a cubic polynomial to the discrete points and use this fit to determine the minimum  $\chi^2$  and the  $1 - \sigma$  interval. In this work, we consider the PDF sets CT10nlo [10], CT14nlo [11], MSTW [12], MMHT [13,14], NNPDF2.3 [15], and NNPDF3.0 [16]. In the ABM [17] PDF set, the correlation between the value of  $\alpha_S(M_Z)$  and the parameters of the PDFs is stronger than in the other PDF set. As a consequence, the  $\chi^2$  dependence on  $\alpha_S(M_Z)$  is much weaker and does not allow for its determination in our fit.

### A. Theoretical prediction

For the theoretical prediction, we used the results of Ref. [9]. In order to perform the extraction procedure and assess uncertainties, we need to reevaluate the same NLO calculation many times with small modifications. We need to evaluate the prediction for a) different values of the renormalization and factorization scales, b) different PDF sets, c) each replica or error set within each PDF set, and d) each value of  $\alpha_S(M_Z)$  provided by the PDF set. This type of repetitive calculation with only minor modifications in the PDF and scale setting was one of the motivations behind the development of the N-TUPLES format for NLO calculations [18]. The other motivation was to allow for the flexibility of defining new observables after the calculation was performed. In our case, we do not require this flexibility, given that we have settled on the histograms we want use, so we can optimize the amount of recalculation needed by using FASTNLO [19] tables. We used the public N-TUPLES provided by the BLACKHAT+SHERPA Collaboration for Z + jets [9] to create FASTNLO grids allowing the fast reevaluation of a fixed set of histograms for a different PDF set and different values of the factorization and renormalization scales.

Due to the finite amount of statistics available in the N-TUPLES, the theoretical predictions have a statistical error. The corresponding covariance matrix can be computed in parallel to the generation of the FASTNLO grids. It includes the correlation between the transverse momentum and rapidity distributions for the same multiplicity. There is

in general a relatively large anticorrelation between neighboring bins due to phase-space points where the real matrix elements and the corresponding subtraction term fall in separate bins. The correlation between other bins is moderate. Since the FASTNLO library does not report statistical integration errors, an alternative method has to be devised to obtain the statistical covariance matrix while avoiding the need to run a full N-TUPLES analysis for each scale and PDF combination. Our strategy is to calculate the statistical covariance matrix for one reference PDF for each scale combination and then rescale the covariance matrix entries for the other members of the set by the ratio of the bin value for the actual  $\alpha_S(M_Z)$  and the reference value:

$$C_{ij}(\alpha_S(M_Z)) \simeq C_{ij}^{\text{ref}} \frac{h_i(\alpha_S(M_Z))}{h_i(\alpha_S^{\text{ref}})} \frac{h_j(\alpha_S(M_Z))}{h_j(\alpha_S^{\text{ref}})}. \quad (3)$$

This approach assumes that the relative correlation between bins is similar between predictions for different values of  $\alpha_S(M_Z)$ . We found this assumption to be true at the level of a few percent for the central choice of scale and assumed it to be valid to the same level of accuracy for the other scale choices. Since the statistical uncertainty of the theoretical prediction is not the dominant term in  $\chi^2$ , this approximation is well justified.

The PDF uncertainty is obtained from the PDF error sets using the LHAPDF library [20]. We evaluated the NLO prediction for each member of the error set and evaluated the covariance matrices according to the prescriptions of Ref. [21] to obtain symmetric errors for the MSTW [12], MMHT [13,14], CT10nlo [10], and CT14nlo [11] PDFs. The covariance matrices of all PDF fits have been rescaled to correspond to a 68% confidence level if necessary. The covariance matrix for NNPDF2.3 [15] and NNPDF3.0 [16] are obtained statistically from the set of 100 replica.

### B. Scale uncertainty

The NLO predictions have been carried out using a factorization and renormalization scale  $\mu_0$  defined in terms of the jet transverse momenta  $p_T^i$  and the mass  $M_Z$  of the Z boson

$$\mu_0 = \hat{H}'_T/2, \quad \hat{H}'_T = \sum_i p_T^i + E_T^Z, \\ E_T^Z = \sqrt{M_Z^2 + (p_T^Z)^2}, \quad (4)$$

where the sum runs over all partons in the final state. To account for the scale uncertainty, we employ two different methods; in both cases, the scale dependence modifies the fit by changing the value of the theoretical prediction in Eq. (1) and the covariance matrix rescaling in Eq. (3). The first method is to repeat the extraction using predictions obtained with factorization and renormalization scales modified from the central scale from Eq. (4)  $\mu_{F,R} = f_{\mu}^{F,R} \mu_0 = f_{\mu}^{F,R} \hat{H}'_T/2$  where the factors  $f_{\mu}^F, f_{\mu}^R$  can be 1/2,

1, 2. The scale uncertainty is taken to be the envelope of the result obtained from all pairs where the factors  $f_\mu^F$  and  $f_\mu^R$  differ by at most a factor of 2.

In the second method, we vary the factorization and renormalization scales by a common factor  $f_\mu = f_\mu^F = f_\mu^R$  and treat the value of this factor as a nuisance parameter for the fit. To do so, we calculate the value of  $\chi^2$  for many different values of  $f_\mu$  and define the profile  $\hat{\chi}^2$ ,

$$\hat{\chi}^2(\alpha_S(M_Z)) = \min_{f_\mu} \chi^2(\alpha_S(M_Z), f_\mu), \quad (5)$$

and then minimize this function  $\hat{\chi}^2(\alpha_S(M_Z))$  as a function of  $\alpha_S(M_Z)$  to obtain the best fit  $\alpha_S(M_Z)$  and  $1 - \sigma$  uncertainty interval. Figure 1 shows the  $\chi^2$  distributions as a function of  $f_\mu$  and  $\alpha_S(M_Z)$  for each PDF set.

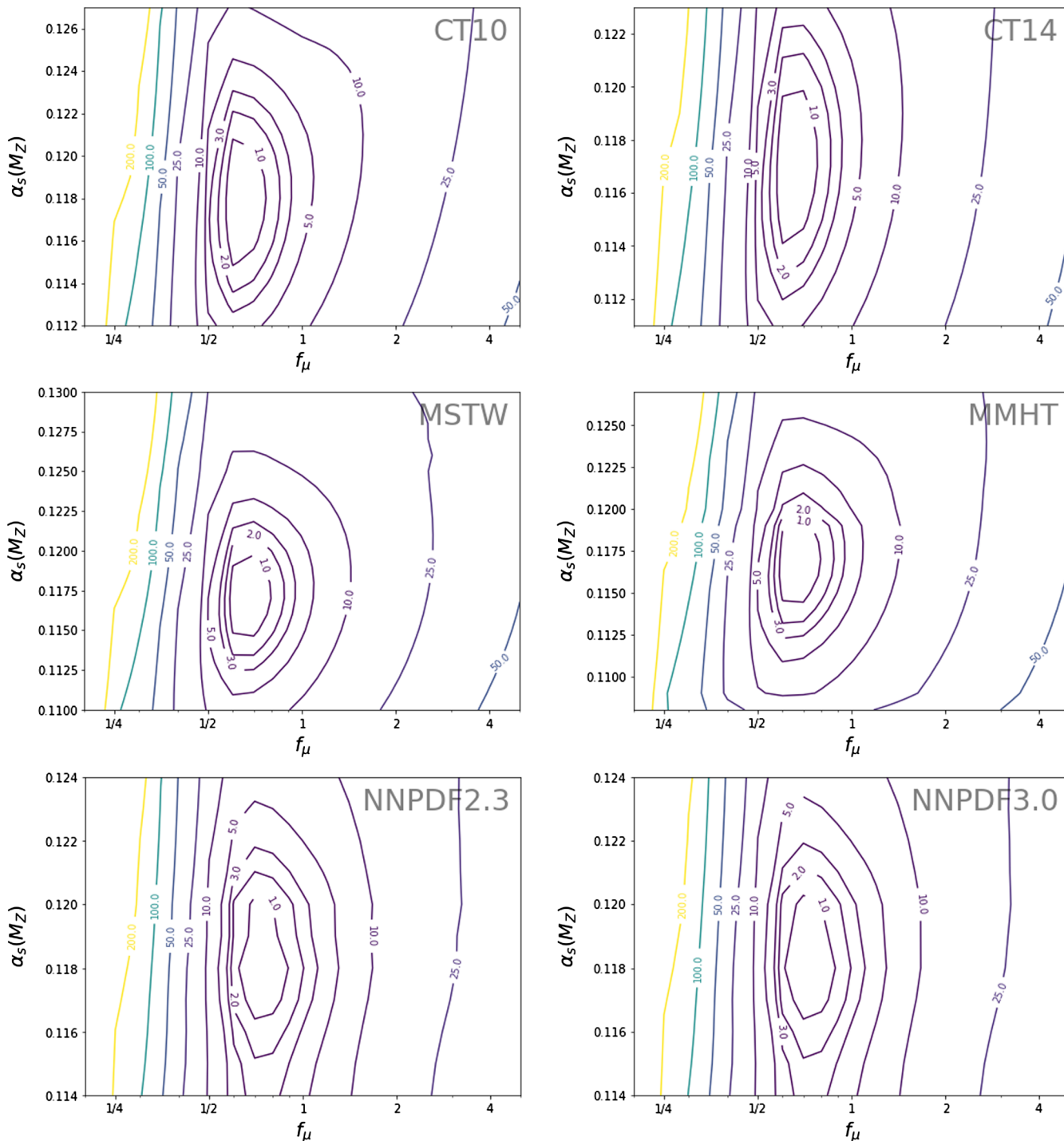


FIG. 1.  $\chi^2$  in the  $\alpha_S(M_Z) - f_\mu$  two-dimensional plane for all the PDF sets considered.

Uncertainty intervals obtained in this way account for both experimental, PDF, and theoretical error sources and also for our choice of  $f_\mu$ . The main advantage of this method is that it does not rely on the somewhat arbitrary values  $f_\mu = 1/2$  and  $f_\mu = 2$  used in the traditional approach. As can be seen from Fig. 1, the fit seems to favor slightly smaller scales than the one used for the central scale.

### C. Nonperturbative corrections

Predictions provided by the BLACKHAT+SHERPA N-TUPLES are at parton level. In order to correct for hadronization and underlying event effects, we corrected the partonic cross section using the same corrections as used in the experimental comparison to the NLO prediction [8]. These nonperturbative corrections are estimated by comparing simulated samples generated using ALPGEN [22] with and without a fragmentation and underlying event model. The correction factors are applied to the theoretical data in Eq. (1) and affect the theoretical covariance matrix through Eq. (3).

In order to assess the uncertainty on these corrections, two independent models are used for the nonperturbative modeling: the first set of corrections uses Herwig+JIMMY [23,24] using the AUET2-CTEQ6L1L tune [25], and the second uses PYTHIA [26] with the PERUGIA2011C tune [27]. In both cases, the correction factors have statistical uncertainty due to the size of the simulated samples used to derive them. This uncertainty is added to the theoretical covariance matrix. As for the scale uncertainty, we use two different methods to estimate the impact of the nonperturbative corrections on our extraction. In the standard method, we use the average of the correction factors for each bin to obtain the central prediction and use the individual correction factors to estimate the uncertainty band. In a more flexible method, we combine the two correction factors according to

$$\delta_{NP} = \lambda \delta_{NP}^{\text{Herwig}} + (1 - \lambda) \delta_{NP}^{\text{Pythia}}. \quad (6)$$

The central value of the standard method described above corresponds to  $\lambda = 1/2$ , and the band is given by the values  $\lambda = 0, 1$ . In the second method, we treat  $\lambda$  as a nuisance parameter. In the tail of the rapidity distributions, the NLO description is not expected to be very accurate, which can be seen in an increase of the corrections described above from a few percent to over 10%. To limit the impact of this corner of phase space to our extraction, we combined the last bins of the rapidity distributions into one bin for each multiplicity in such a way that the correction factor for the resulting bin does not exceed 10%.

### D. Experimental data

The experimental values we used in this extraction were obtained from measurements of jets produced in association with a  $Z$  boson in proton-proton collisions at a center-of-mass energy  $\sqrt{s} = 7$  TeV. The data correspond to an integrated luminosity of  $4.6 \text{ fb}^{-1}$  collected by the ATLAS detector. The  $Z$  bosons were selected in the electron and muon pair decay channels with an invariant mass window for the lepton pair  $66 \text{ GeV} \leq m_{l+l-} \leq 116 \text{ GeV}$ . The jets were selected with a transverse momentum cut of  $p_T > 30 \text{ GeV}$  and a rapidity cut  $|y| < 4.4$ . For our fits, we used the combination of the electron and muon channels where the leptons are selected with  $p_T > 20 \text{ GeV}$  and  $|\eta| < 2.5$ .

For our  $\alpha_s$  extraction, we use the results presented in Ref. [28] and available from HEPDATA [29,30] for the rapidity and transverse momentum distribution of the  $n$ th jet in inclusive  $Z + n$  jets event samples. We corrected the results for the updated total luminosity reported in Ref. [31]. The experimental uncertainties can be separated into three categories: the statistical error, the systematic uncertainty, and the luminosity uncertainty. The authors used the procedure described in Refs. [32,33] to separate

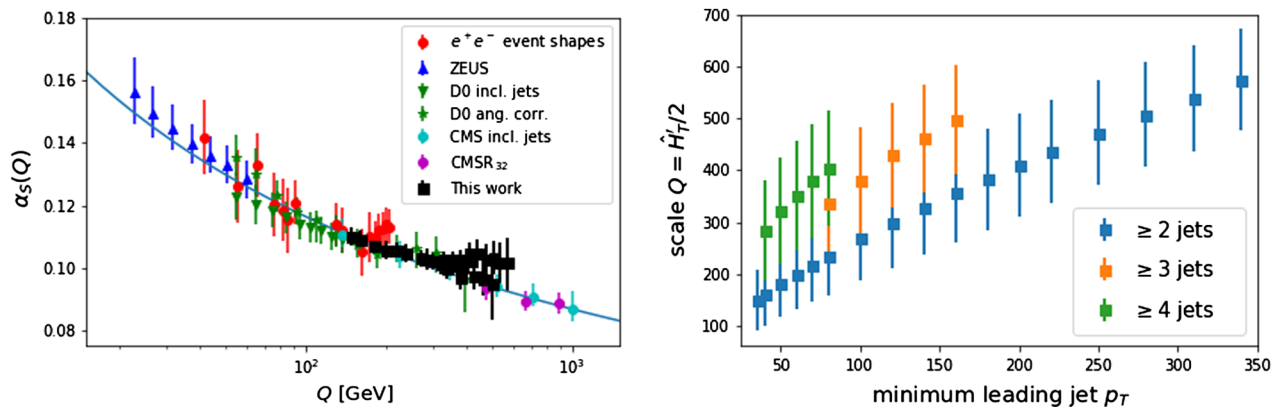


FIG. 2. Left panel: Measurement of the strong coupling constant as a function of  $Q^2$ . The error bars represent the experimental and PDF uncertainties and the statistical error of the theory prediction but do not include the scale and nonperturbative uncertainties. Right panel: Expectation value of  $Q^2$  as a function of the minimum jet transverse momentum considered for the fit. The PDF set MSTW2008 [35] was used for these two figures.

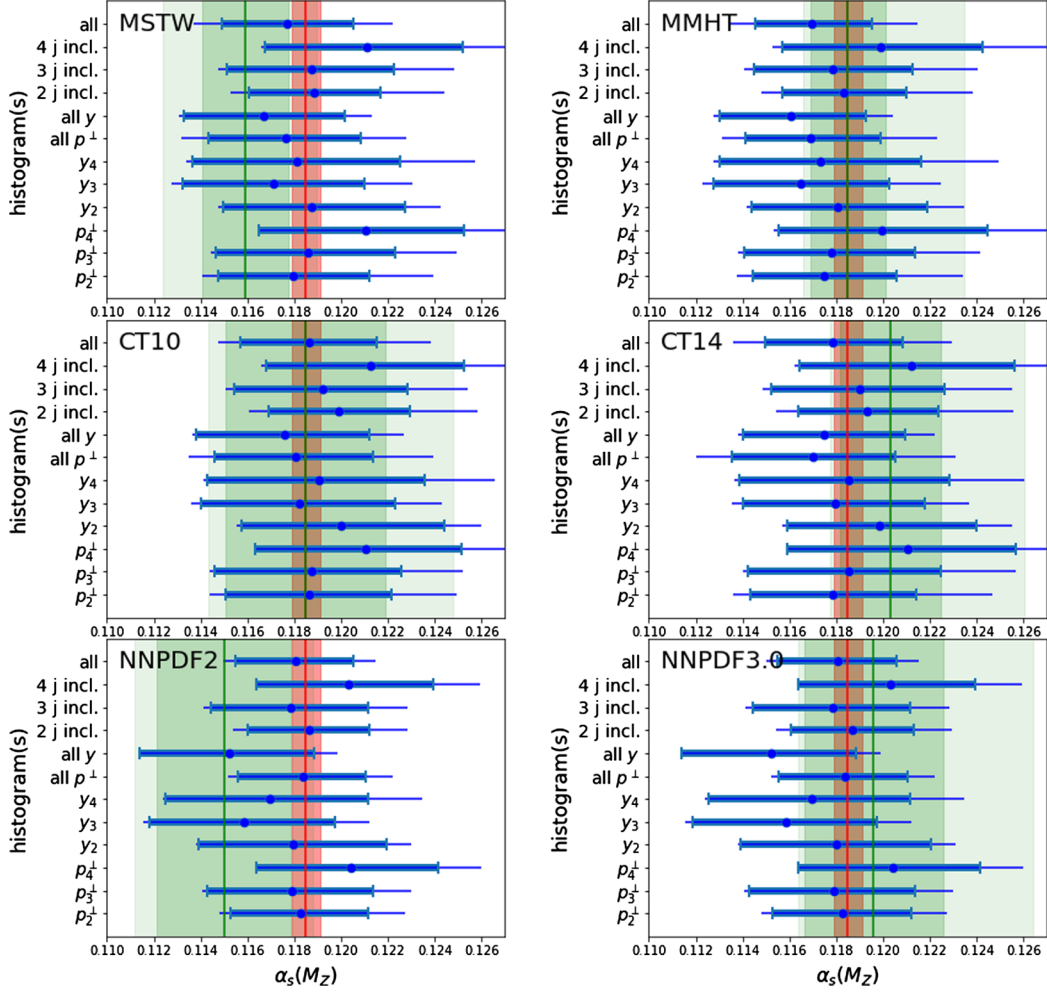


FIG. 3. Strong coupling values for different PDF sets for each considered histogram and combinations listed in Table I. The green bands on the left-hand plots are the result from Ref. [4], and the green bands on the right-hand side show the results from Ref. [3]. (The NNPDF results from Ref. [4] used version 2.1, while we used version 2.3 in this work.) The darker regions represent the uncertainties without the scale variation, and the lighter regions show the total uncertainties including the scale variation. The red band is the world average [1]. The boundaries of the thick part of the error bars represent the values of  $\alpha_s(M_Z)$  for which the  $\chi^2 - \chi^2_{\min} = 1$ . These error estimates do not include scale variation. The thin error bars show the uncertainty including the scale uncertainties.

the correlated uncertainties into a set of independent fully correlated uncertainties which we used to calculate the full experimental covariance matrix. The resulting covariance matrix shows a large correlation between all rapidity bins, both within the same distribution and between bins in distributions for different jet multiplicity samples. Low transverse momentum bins are strongly correlated both with themselves and with the rapidity bins. Higher transverse momentum bins show a lower correlation both to low transverse momentum bins and to rapidity bins.

### III. RESULTS

The left panel of Fig. 2 shows the scale dependence of  $\alpha_s(Q)$ . The different points on the graph represent the

TABLE I. Observables and labels for the fits.

Label	Observable(s)
all	Combination of all histograms
2j, incl	Combination of the transverse momentum and rapidity of the second jet for the two-jet inclusive sample
3j, incl	Combination of the transverse momentum and rapidity of the third jet for the three-jet inclusive sample
4j, incl	Combination of the transverse momentum and rapidity of the fourth jet for the four-jet inclusive sample
all y	Combination of all the rapidity distributions
all $p^\perp$	Combination of all three transverse momentum distributions
$y_i$	Rapidity for the $i$ -jet inclusive sample
$p_i^\perp$	Transverse momentum for the $i$ -jet inclusive sample

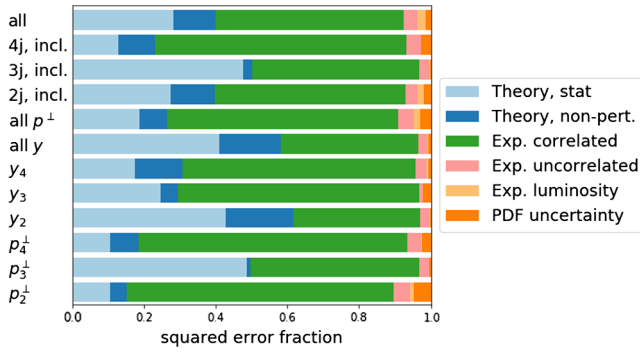


FIG. 4. Share of the uncertainty by error source according to Eq. (7) for each combination listed in Table I. The results are for the PDF set CT14.

value of  $\alpha_S$  obtained by performing a dedicated fit to the transverse momentum distribution of the  $i$ th jet but restricting the fit to a subset of bins above a given threshold. Since the jet transverse momentum is correlated with the scale  $\mu_0$ , raising the minimum transverse momentum considered in the fit effectively probes the strong coupling constant at higher scales. The value of the scale  $Q$  assigned to the fit value is the expectation value of the scale used for the NLO calculation ( $\mu_0 = \hat{H}'_T/2$  as defined in Ref. [34]) for the subset of bins satisfying the minimum jet transverse momentum requirement. These scales are shown in the right panel of Fig. 2 for each multiplicity as a function of the minimum transverse momentum in the bin subset. The error bars represent the variance of scale when restricted to the bins above the minimum transverse momentum. The values shown in Fig. 2 are obtained using the CT10nlo PDF set, and the values obtained with other PDF sets are very similar. The values that fall somewhat above the theoretical curve correspond to the highest values of the second jet  $p_{2,\min}^T$ . In this very restricted phase space, the three- and four-jets contributions are significant so that the NLO two-jet calculation underestimates the cross section, resulting in a higher  $\alpha_S(M_Z)$  value.

The left-hand column of plots in Fig. 3 shows the best fit results for the PDF sets MSTW2008 [35], CT10 [36] and NNPDF2.3 [15]. These sets were chosen to facilitate the comparison with the results obtained in Ref. [4]. The

right-hand column of plots in Fig. 3 shows the best fit results for the PDF sets MMHT [13], CT14 [11] and NNPDF3.0 [16]. The results for this set of PDFs are compared with the results published in Ref. [3]. The results are given for fits to the combinations of observables listed in Table I. A few patterns emerge from Fig. 3:

- The fit to the rapidity histograms favors smaller values of  $\alpha_S(M_Z)$ , while fits to the rapidity distributions prefer larger values of  $\alpha_S(M_Z)$ .
- Fits for the lower multiplicities tend to yield only moderately more accurate results than higher-multiplicity ones.
- The covariance matrix for the rapidity distributions displays a large correlation, causing their combination to yield a value more extreme than any individual result.

To estimate the share of the uncertainties due to each error source, we use the quantities

$$\chi_s^2 = (y_t(\alpha_s(M_Z)) - y_d)^T C_{\text{tot}}^{-1} C_s C_{\text{tot}}^{-1} (y_t(\alpha_s(M_Z)) - y_d) \quad (7)$$

defined for each error source covariance matrix  $C_s$ . The  $\chi_s^2$  sum up to the total  $\chi^2$ . We assign each error source a fraction  $\chi_s^2/\chi^2$  of the total uncertainty. In the limit where all errors are fully uncorrelated, this procedure is equivalent to summing the errors in quadrature. Figure 4 shows an example of how the uncertainty is shared between the error sources for CT14. The figure shows the share for each individual distribution, for the combination of all transverse momentum distributions and rapidities, for the multiplicity combination, and for the full combination. We can see that the dominant share of the uncertainty comes from the experimental uncertainties. In principle, the uncertainty could be reduced by increasing the statistical accuracy of the theory prediction and the understanding of the non-perturbative corrections.

Table II shows the result for the best fit  $\alpha_S(M_Z)$  for a list of PDF sets. The uncertainties in this table do not include scale variation and nonperturbative correction uncertainties. The theory and experimental uncertainties are approximately the same size, while the PDF uncertainty is almost one order of magnitude smaller. The  $\chi^2$  per degree of freedom is slightly below 1 and is very similar across PDF sets.

TABLE II. Results for the coupling constant extraction with uncertainties.

PDF set	$\alpha_S(M_Z)$	Uncertainties detail	$\chi^2/\text{ndof}$
CT10nlo	$0.1186^{+0.0029}_{-0.0029}$	$+0.0018$ (theory) $+0.0022$ (exp) $+0.00035$ (pdf) $-0.0018$ (theory) $-0.0023$ (exp) $-0.00036$ (pdf)	45.4/60
MSTW2008nlo68cl	$0.1177^{+0.0028}_{-0.0028}$	$+0.0017$ (theory) $+0.0022$ (exp) $+0.00034$ (pdf) $-0.0017$ (theory) $-0.0022$ (exp) $-0.00034$ (pdf)	48.5/60
NNPDF2.3_nlo_as_0118	$0.1180^{+0.0025}_{-0.0025}$	$+0.0016$ (theory) $+0.0019$ (exp) $+0.00022$ (pdf) $-0.0016$ (theory) $-0.0020$ (exp) $-0.00022$ (pdf)	46.5/60
CT14nlo	$0.1178^{+0.0030}_{-0.0029}$	$+0.0019$ (theory) $+0.0023$ (exp) $+0.00042$ (pdf) $-0.0018$ (theory) $-0.0022$ (exp) $-0.00041$ (pdf)	46.7/60
MMHT2014nlo	$0.1169^{+0.0026}_{-0.0024}$	$+0.0016$ (theory) $+0.0020$ (exp) $+0.00032$ (pdf) $-0.0015$ (theory) $-0.0019$ (exp) $-0.00029$ (pdf)	47.8/60
NNPDF3.0_nlo_as_0118	$0.1181^{+0.0025}_{-0.0026}$	$+0.0016$ (theory) $+0.0019$ (exp) $+0.00025$ (pdf) $-0.0016$ (theory) $-0.0020$ (exp) $-0.00025$ (pdf)	46.3/60

TABLE III. Scale uncertainties for the  $\alpha_s(M_Z)$  extraction. The first column repeats the result of Table II for the theoretical, experimental, and PDF uncertainties from the fit. The second and third columns show the uncertainties resulting from varying the scale by either correlated or uncorrelated factors. The fourth column shows the result of the fit in which the scale factor is treated as a nuisance parameter. The last column shows the value of  $f_\mu$  corresponding to the best fit.

PDF set	$\alpha_s(M_Z)$	Scale correlated	Scale uncorrelated	$f_\mu$ as nuisance parameter	Preferred $f_\mu$
CT10nlo	$0.1186^{+0.0029}_{-0.0029}$	$+0.0039$ $-0.0018$	$+0.0039$ $-0.0018$	$0.1180^{+0.0030}_{-0.0031}$	0.63
MSTW2008nlo68cl	$0.1177^{+0.0028}_{-0.0028}$	$+0.0023$ $-0.0021$	$+0.0027$ $-0.0021$	$0.1170^{+0.0029}_{-0.0028}$	0.67
NNPDF2.3_nlo_as_0118	$0.1180^{+0.0025}_{-0.0025}$	$+0.0017$ $-0.0006$	$+0.0017$ $-0.0006$	$0.1179^{+0.0025}_{-0.0026}$	0.73
CT14nlo	$0.1178^{+0.0030}_{-0.0029}$	$+0.0031$ $-0.0025$	$+0.0034$ $-0.0025$	$0.1170^{+0.0031}_{-0.0030}$	0.64
MMHT2014nlo	$0.1169^{+0.0026}_{-0.0024}$	$+0.0027$ $-0.0019$	$+0.0030$ $-0.0019$	$0.1163^{+0.0025}_{-0.0023}$	0.67
NNPDF3.0_nlo_as_0118	$0.1181^{+0.0025}_{-0.0026}$	$+0.0017$ $-0.0003$	$+0.0017$ $-0.0003$	$0.1180^{+0.0025}_{-0.0026}$	0.72

TABLE IV. Nonperturbative uncertainty for the  $\alpha_s(M_Z)$  extraction. The results in first column are obtained by correcting each bin with the average of the correction factors obtained with ALPGEN+Herwig and ALPGEN+Pythia. The second and third columns are the results obtained using only the individual programs. The last column is the uncertainty, taken as the difference between the central values and the second and third columns.

PDF set	Central value	ALPGEN+Herwig	ALPGEN+Pythia	Uncertainty
CT10nlo	0.1186	0.1205	0.1168	$+0.0018$ $-0.0018$
MSTW2008nlo68cl	0.1177	0.1199	0.1158	$+0.0022$ $-0.0019$
NNPDF2.3_nlo_as_0118	0.1180	0.1198	0.1164	$+0.0017$ $-0.0017$
CT14nlo	0.1178	0.1202	0.1159	$+0.0023$ $-0.0019$
MMHT2014nlo	0.1169	0.1192	0.1154	$+0.0023$ $-0.0016$
NNPDF3.0_nlo_as_0118	0.1181	0.1197	0.1164	$+0.0017$ $-0.0017$

Table III shows scale variation uncertainty estimates using the two methods outlined in Sec. II B. The second and third columns vary the factorization and renormalization scales by factors of 1/2, 1, or 2. The second column shows the resulting uncertainty if the same factor is chosen for both scales, and the third column shows the uncertainty resulting from choosing any two factors differing by at

most a factor of 2. Comparing these two columns, we can see that the correlated variation covers most of the range of the uncorrelated variation.

While the  $1 - \sigma$  intervals from the  $\chi^2$  fit are essentially symmetric, the uncertainties due to the first scale variation method are asymmetric, with the upward fluctuation generally much larger than the downward one. Using the nuisance parameter approach to scale variation, we get roughly symmetric uncertainty estimates and lower best fit values. The uncertainty interval is marginally smaller for MMHT2014 but larger for all other PDF sets. This approach gives more symmetric error intervals than the standard variation, as in the case of NNPDF2.3 in which the standard variation gave a very small lower variation in the standard approach. The last column of Table III shows the value of  $f_\mu$  corresponding to the lowest  $\chi^2$ . It is lower than 1 for all PDF sets but larger than 1/2, so these values of  $f_\mu$  are within the range of values considered in the traditional scale variation approach.

Table IV collects the results for the assessment of the nonperturbative corrections. Using the correction factors calculated using ALPGEN+Herwig leads to higher values of  $\alpha_s(M_Z)$  than when using ALPGEN+Pythia. The difference between the results obtained with the two sets of programs is quite large and is commensurate with the other

TABLE V. Summary of the extraction uncertainty. The second column lists the best fit value of the fit with the associated uncertainties. The third and fourth columns show the estimates of the nonperturbative and scale uncertainties using the standard method. The last column shows the result of a fit in which both the scale factor and the relative weight of the correction factors are treated as nuisance parameters.

PDF set	Total (standard)	Total (nuisance)
CT10nlo	$0.1186^{+0.0029}_{-0.0029}$ (fit) $+0.0018$ (NP) $+0.0039$ (scale) = $0.1186^{+0.0052}_{-0.0039}$	$0.1177^{+0.0037}_{-0.0041}$
MSTW2008nlo68cl	$0.1177^{+0.0028}_{-0.0028}$ (fit) $+0.0022$ (NP) $+0.0027$ (scale) = $0.1177^{+0.0045}_{-0.0040}$	$0.1177^{+0.0036}_{-0.0038}$
NNPDF2.3_nlo_as_0118	$0.1180^{+0.0025}_{-0.0025}$ (fit) $+0.0017$ (NP) $+0.0017$ (scale) = $0.1180^{+0.0035}_{-0.0031}$	$0.1197^{+0.0025}_{-0.0031}$
CT14nlo	$0.1178^{+0.0030}_{-0.0029}$ (fit) $+0.0023$ (NP) $+0.0034$ (scale) = $0.1178^{+0.0051}_{-0.0043}$	$0.1160^{+0.0044}_{-0.0037}$
MMHT2014nlo	$0.1169^{+0.0026}_{-0.0024}$ (fit) $+0.0023$ (NP) $+0.0030$ (scale) = $0.1169^{+0.0046}_{-0.0034}$	$0.1166^{+0.0030}_{-0.0028}$
NNPDF3.0_nlo_as_0118	$0.1181^{+0.0025}_{-0.0026}$ (fit) $+0.0017$ (NP) $+0.0017$ (scale) = $0.1181^{+0.0034}_{-0.0031}$	$0.1197^{+0.0026}_{-0.0031}$

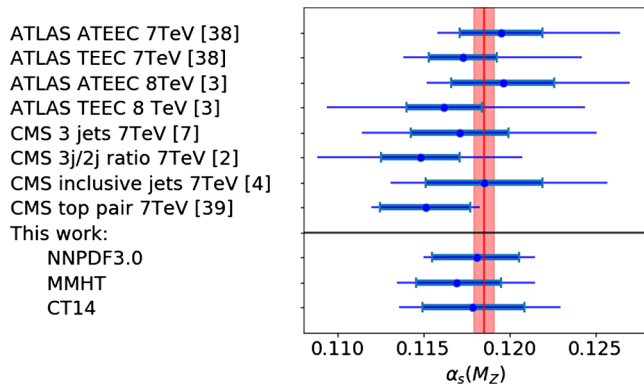


FIG. 5. Comparison of the results presented in this work and other strong coupling extractions using LHC data. The thick part of the error bar includes all errors but the scale uncertainty. The narrow part of the error bar takes that uncertainty into account. TEEC stands for transverse energy-energy correlation, and ATEEC stands for its asymmetry.

uncertainties affecting the fit. Such a large disagreement in the values of nonperturbative corrections is not uncommon; see, for example, Refs. [3,37].

The results of our extraction are summarized in Table V. The first columns show the results using the standard approach to estimating the scale and nonperturbative uncertainties, while the last column shows the result of the approach in which both the scale factor and

the mixing parameter  $\lambda$  in Eq. (6) are treated as nuisance parameters in the fit. Treating the scale factor and the nonperturbative mixing parameter  $\lambda$  as nuisance parameters leads to a smaller value of  $\alpha_s(M_Z)$  for all PDF sets except for the NNPDF sets in which the best fit value increases. The uncertainty intervals are smaller for NNPDF2.3, NNPDF3, CT14, and CT10 but larger for MSTW and MMHT.

Figure 5 shows our results alongside other extractions of  $\alpha_s(M_Z)$  [2–4,7,38,39] using LHC data. In general, our results have comparable experimental uncertainties. With the exception of the CMS extraction from  $t\bar{t}$  production, the result we obtained displays a smaller scale uncertainty than the other extractions using LHC data. This observation can be explained by the fact that at NLO the scale uncertainty does not increase with a constant multiplicative factor with each additional power of the coupling constant. This is an important advantage of using high-multiplicity processes to extract a measurement of  $\alpha_s(M_Z)$  since adding more experimental data and improving the experimental uncertainties will improve the accuracy of the extraction significantly, while the accuracy of other methods is already limited by the scale contribution to the overall uncertainty. For our final result, we choose the value obtained using CT14, using the conventional scale and nonperturbative uncertainty estimation method as they result in the most conservative result:

$$\begin{aligned} \alpha_s(M_Z) &= 0.1178_{-0.0018}^{+0.0019}(\text{theory})_{-0.0022}^{+0.0023}(\text{exp})_{-0.00041}^{+0.00042}(\text{pdf})_{-0.0025}^{+0.0034}(\text{scale}) \\ &= 0.1178_{-0.0029}^{+0.0030}(\text{all but scale})_{-0.0025}^{+0.0034}(\text{scale}) \\ &= 0.1178_{-0.0043}^{+0.0051}. \end{aligned}$$

#### IV. CONCLUSION

We presented an extraction of the strong coupling constant from high-multiplicity  $Z + \text{jets}$  processes. Our most conservative result is  $\alpha_s(M_Z) = 0.1178_{-0.0043}^{+0.0051}$ , obtained with the CT14 PDF set. Table V and Fig. 5 summarize the best fit values and uncertainty estimates for other PDF sets. We used two different methods to assert the uncertainties from the scale variation and the nonperturbative corrections. Both methods yield comparable results. The best fit value for  $\alpha_s(M_Z)$  is in good agreement with the current world average value, and its uncertainty is comparable to other NLO determinations at the LHC but have a smaller scale uncertainty and a larger experimental uncertainty.

The results we obtained show the potential of high-multiplicity processes for the extraction of the strong coupling constant: the larger experimental uncertainties are mostly compensated by the steeper dependence on  $\alpha_s(M_Z)$ . The lower multiplicities have slightly smaller

uncertainties, but the higher-multiplicity processes still contribute to the reduction of the final uncertainty. Our results highlight another advantage of higher-multiplicity processes: as they have a relatively smaller scale uncertainty, they provide complementary information to other measurements at the LHC for which the scale variation is the major source of uncertainty.

The lowest hanging fruit to improve on the uncertainty of the results is to improve the statistical precision of the theoretical prediction. The extraction can be improved with the larger statistics of more recent runs at the LHC and a reduction in the systematic errors of the measurement. A better understanding of nonperturbative effects will also improve the accuracy of the extraction significantly. It is reasonable to expect improvements on all these fronts in the future so we can expect large-multiplicity processes to provide improved constraints on the value of the strong coupling constant.

## ACKNOWLEDGMENTS

We would like to thank Nigel Glover, Klaus Rabbertz, and Stefano Forte for useful discussions, and we are grateful to Ulla Blumenschein for providing the nonperturbative corrections used in this work before their publication and for her help with the experimental uncertainties.

- 
- [1] K. A. Olive *et al.* (Particle Data Group Collaboration), *Chin. Phys. C* **38**, 090001 (2014).
- [2] S. Chatrchyan *et al.* (CMS Collaboration), *Eur. Phys. J. C* **73**, 2604 (2013).
- [3] M. Aaboud *et al.* (ATLAS Collaboration), *Eur. Phys. J. C* **77**, 872 (2017).
- [4] V. Khachatryan *et al.* (CMS Collaboration), *Eur. Phys. J. C* **75**, 288 (2015).
- [5] R. Frederix, S. Frixione, K. Melnikov, and G. Zanderighi, *J. High Energy Phys.* **11** (2010) 050.
- [6] N. Brambilla, X. G. i Tormo, J. Soto, and A. Vairo, *Phys. Rev. D* **75**, 074014 (2007).
- [7] V. Khachatryan *et al.* (CMS Collaboration), *Eur. Phys. J. C* **75**, 186 (2015).
- [8] G. Aad *et al.* (ATLAS Collaboration), *Phys. Rev. D* **85**, 032009 (2012).
- [9] H. Ita, Z. Bern, L. J. Dixon, F. Febres Cordero, D. A. Kosower, and D. Maître, *Phys. Rev. D* **85**, 031501 (2012).
- [10] H.-L. Lai, M. Guzzi, J. Huston, Z. Li, P. M. Nadolsky, J. Pumplin, and C.-P. Yuan, *Phys. Rev. D* **82**, 074024 (2010).
- [11] S. Dulat, T.-J. Hou, J. Gao, M. Guzzi, J. Huston, P. Nadolsky, J. Pumplin, C. Schmidt, D. Stump, and C. P. Yuan, *Phys. Rev. D* **93**, 033006 (2016).
- [12] A. Martin, W. Stirling, R. Thorne, and G. Watt, *Eur. Phys. J. C* **63**, 189 (2009).
- [13] L. A. Harland-Lang, A. D. Martin, P. Motylinski, and R. S. Thorne, *Eur. Phys. J. C* **75**, 204 (2015).
- [14] L. A. Harland-Lang, A. D. Martin, P. Motylinski, and R. S. Thorne, *Eur. Phys. J. C* **75**, 435 (2015).
- [15] R. D. Ball *et al.*, *Nucl. Phys.* **B867**, 244 (2013).
- [16] R. D. Ball *et al.* (NNPDF Collaboration), *J. High Energy Phys.* **04** (2015) 040.
- [17] S. Alekhin, J. Blumlein, and S. Moch, *Phys. Rev. D* **86**, 054009 (2012).
- [18] Z. Bern, L. J. Dixon, F. F. Cordero, S. Höche, H. Ita, D. A. Kosower, and D. Maître, *Comput. Phys. Commun.* **185**, 1443 (2014).
- [19] D. Britzger, K. Rabbertz, F. Stober, and M. Wobisch (fastNLO Collaboration), in *Proceedings, 20th International Workshop on Deep-Inelastic Scattering and Related Subjects (DIS 2012)* (DESY, Germany, 2012), p. 217.
- [20] M. R. Whalley, D. Bourilkov, and R. C. Group, [arXiv: hep-ph/0508110](https://arxiv.org/abs/hep-ph/0508110).
- [21] G. Watt and R. S. Thorne, *J. High Energy Phys.* **08** (2012) 052.
- [22] M. L. Mangano, M. Moretti, F. Piccinini, R. Pittau, and A. D. Polosa, *J. High Energy Phys.* **07** (2003) 001.
- [23] G. Corcella, I. G. Knowles, G. Marchesini, S. Moretti, K. Odagiri, P. Richardson, M. H. Seymour, and B. R. Webber, *J. High Energy Phys.* **01** (2001) 010.
- [24] J. M. Butterworth, J. R. Forshaw, and M. H. Seymour, *Z. Phys. C* **72**, 637 (1996).
- [25] ATLAS collaboration, Report No. ATL-PHYS-PUB-2011-008, 2011.
- [26] T. Sjostrand, S. Mrenna, and P. Z. Skands, *J. High Energy Phys.* **05** (2006) 026.
- [27] P. Z. Skands, *Phys. Rev. D* **82**, 074018 (2010).
- [28] G. Aad *et al.* (ATLAS Collaboration), *J. High Energy Phys.* **07** (2013) 032.
- [29] <http://www.hepdata.net/record/ins1230812>.
- [30] E. Maguire, L. Heinrich, and G. Watt, *J. Phys.: Conf. Ser.* **898**, 102006 (2017).
- [31] G. Aad *et al.* (ATLAS Collaboration), *Eur. Phys. J. C* **73**, 2518 (2013).
- [32] G. Aad *et al.* (ATLAS Collaboration), *Eur. Phys. J. C* **73**, 2304 (2013).
- [33] ATLAS collaboration, Report No. ATLAS-CONF-2013-004.
- [34] Z. Bern, L. J. Dixon, F. F. Cordero, S. Höche, H. Ita, D. A. Kosower, D. Maître, and K. Ozeren, *Phys. Rev. D* **88**, 014025 (2013).
- [35] A. Martin, W. Stirling, R. Thorne, and G. Watt, *Eur. Phys. J. C* **63**, 189 (2009).
- [36] J. Gao, M. Guzzi, J. Huston, H.-L. Lai, Z. Li, P. Nadolsky, J. Pumplin, D. Stump, and C. P. Yuan, *Phys. Rev. D* **89**, 033009 (2014).
- [37] M. Aaboud *et al.* (ATLAS Collaboration), *J. High Energy Phys.* **09** (2017) 020.
- [38] G. Aad *et al.* (ATLAS Collaboration), *Phys. Lett. B* **750**, 427 (2015).
- [39] S. Chatrchyan *et al.* (CMS Collaboration), *Phys. Lett. B* **728**, 496 (2014); **738**, 526(E) (2014).